AMERICAN SOCIETY FOR MICROBIOLOGY | Journal of Virology®

VIRUS-CELL INTERACTIONS

Viral Nonstructural Protein 1 Induces Mitochondrion-Mediated Apoptosis in Mink Enteritis Virus Infection

Peng Lin,[a,b,c] Yuening Cheng,[a] Shanshan Song,[a] Jianming Qiu,[d] Li Yi,[a] Zhigang Cao,[a] Jianrong Li,[b,c] Shipeng Cheng,[a] Jianke Wang[a]

[a]Key Laboratory of Special Animal Epidemic Disease, Institute of Special Animal and Plant Sciences, Chinese Academy of Agricultural Sciences, Changchun, China
[b]National and Local Joint Engineering Research Center of Storage, Processing and Safety Control Technology for Fresh Agricultural and Aquatic Products, Bohai University, Jinzhou, China
[c]Fresh Food Storage and Processing Technology Research Institute of Liaoning Provincial Universities, Bohai University, Jinzhou, China
[d]Department of Microbiology, Molecular Genetics and Immunology, University of Kansas Medical Center, Kansas City, Kansas, USA

ABSTRACT Mink enteritis virus (MEV), an autonomous parvovirus, causes acute hemorrhagic enteritis in minks. The molecular pathogenesis of MEV infection has not been fully understood. In this study, we observed significantly increased apoptosis in the esophagus, small intestine, mesenteric lymph nodes, and kidney in minks experimentally infected with strain MEVB. *In vitro* infection of feline F81 cells with MEVB decreased cell viability and induced cell cycle arrest at G_1 phase and apoptosis. By screening MEV nonstructural proteins (NS1 and NS2) and structural proteins (VP1 and VP2), we demonstrated that the MEV NS1 induced apoptosis in both F81 and human embryonic kidney 293T (HEK293T) cells, similar to that induced during MEV infection in minks. We found that the NS1 protein-induced apoptosis in HEK293T cells was mediated not by the death receptor but by the mitochondrial pathway, as demonstrated by mitochondrial depolarization, opening of mitochondrial transition pore, release of cytochrome *c*, and activation of caspase-9 and -3. Moreover, in *NS1*-transfected cells, we observed an increase of Bax expression and its translocation to the mitochondria, as well as an increased ratio of the Bax/Bcl-2, reactive oxygen species (ROS) production, and activated p38 mitogen-activated protein kinase (MAPK) and p53. Taken together, our results demonstrated that MEV induces apoptosis through activation of p38 MAPK and the p53-mediated mitochondrial apoptotic pathway induced by NS1 protein, which sheds light on the molecular pathogenesis of MEV infection.

IMPORTANCE MEV causes fatal hemorrhagic enteritis in minks. Apoptosis is a cellular mechanism that effectively sacrifices virus-infected cells to maintain homeostasis between the virus and host. In this study, we demonstrated that MEV induces apoptosis both *in vivo* and *in vitro*. Mechanistically, the viral large nonstructural protein NS1 activates p38 MAPK, which leads p53 phosphorylation to mediate the mitochondrial apoptotic pathway but not the death receptor-mediated apoptotic pathway. This is the first report to uncover the mechanism underlying MEV-induced apoptosis.

KEYWORDS parvovirus, NS1 protein, apoptosis, caspase, mitochondrial apoptotic pathways, mink enteritis virus

Cell death can either be regulated (i.e., programmed cell death [PCD]) or unprogrammed, known as necrosis (1). PCD is a genetically regulated physiological process that is indispensable for maintenance of tissue homeostasis as well as embryogenesis and development (2). PCD can be mediated via apoptosis, named type I cell death, or autophagy, named type II cell death (3). Apoptosis is triggered by various

Citation Lin P, Cheng Y, Song S, Qiu J, Yi L, Cao Z, Li J, Cheng S, Wang J. 2019. Viral nonstructural protein 1 induces mitochondrion-mediated apoptosis in mink enteritis virus infection. J Virol 93:e01249-19. https://doi.org/10.1128/JVI.01249-19.

Editor Jae U. Jung, University of Southern California

Address correspondence to Jianke Wang, wangjianke@caas.cn.

Received 8 August 2019
Accepted 26 August 2019
Accepted manuscript posted online 4 September 2019
Published 29 October 2019

stimuli, including virus infections, starvation, and cytotoxic agents. Apoptosis is mediated by death receptor and mitochondrial or endoplasmic reticulum (ER) stress pathways that lead to activation of the caspases. Many RNA and DNA viruses, including influenza A virus, rabies virus, transmissible gastroenteritis virus, and porcine reproductive and respiratory syndrome virus, have adopted strategies to promote survival and evade the host cell immune response that leads to apoptosis (4–7).

Mink enteritis virus (MEV), a member of the genus *Protoparvovirus* of the *Parvoviridae* family (8, 9), causes fatal hemorrhagic enteritis in minks (10). MEV has a negative-sense single-stranded DNA genome, which contains two open reading frames (ORFs) that encode two nonstructural proteins (NS1 and NS2) and two capsid proteins (VP1 and VP2) (11, 12). During parvovirus infection, apoptosis is one of the important pathogenic mechanisms leading to cell or tissue damage (13). Porcine parvovirus (PPV), rat parvovirus (H-1PV), canine parvovirus (CPV), minute virus of canines (MVC), and human parvovirus B19 have been extensively studied for their apoptosis properties (14–18).

The large nonstructural protein of parvovirus, NS1, is a multifunctional protein that is critical for viral replication and cytotoxicity. NS1 proteins of several parvoviruses have been reported to cause cell cycle arrest and initiate apoptosis (11, 16, 19). The NS1 of the CPV-2 causes cell cycle arrest, accumulation of reactive oxygen species (ROS), and activation of the mitochondrial apoptotic pathway (20). NS1 of H-1 parvovirus induces apoptosis via the accumulation of cells at G_2 phase and the activation of caspase-9 and -3 (11). Similarly, NS1 of human parvovirus B19 causes cell cycle arrest at G_2 phase and induces apoptosis through the activation of caspases (21–24). NS1 of minute virus of mice (MVM) alters the cytoskeletal structures of both transformed and cancer cells, which causes cell death (12, 25).

Nevertheless, little is known about the mechanisms underlying MEV-induced cell death. In this study, we investigated the cell death induced by MEV infection in animals and cells, as well as the cell death induced by NS1 in transfected cells. We observed that MEV NS1 induces apoptosis through the activation of p38 mitogen-activated protein kinase (MAPK) and p53 signaling that leads to the mitochondrion-mediated pathway.

RESULTS

MEV infection induces apoptosis in various tissues of infected minks. In order to examine the nature of MEV infection-caused cell death in animals, we chose 10-week-old healthy minks for infection. At 2 to 4 days postinfection, all inoculated minks exhibited anorexia and depression, followed by diarrhea and/or vomiting, lethargy, and dehydration. The most severe diarrhea was exhibited at 5 days postinfection. All the minks died at approximately 7 days postinfection. No abnormalities were found in the uninfected (mock) group. We then used *in situ* terminal deoxynucleotidyltransferase-mediated dUTP-biotin nick end labeling (TUNEL) staining to analyze apoptosis in singly or serially cut tissue sections from the esophagus, small intestine, mesenteric lymph nodes, and kidneys of the minks. Most of the TUNEL-positive cells were detected in the esophagus, small intestine, mesenteric lymph nodes, and kidneys of the infected minks, whereas a few *in situ* TUNEL-positive cells were occasionally detected in the negative group (Fig. 1A). Compared to that in the mock-infected group, the apoptosis in esophagus, small intestine, mesenteric lymph nodes, and kidney increased significantly in the MEV-infected group (Fig. 1B). Collectively, our results revealed that MEV induces apoptosis in various tissues of the digestive tract of infected minks.

MEV infection induces apoptosis in feline F81 cells. Previous research demonstrated that MEV replication induced morphological alterations and lysis in infected cells. We asked whether MEV infection induced apoptosis in MEV-permissive F81 feline cells. At 24 h postinfection, significant inhibition of cellular viability appeared in F81 cells infected with MEVB, which became more evident during the course of infection (Fig. 2A). We then analyzed the cell cycle of MEVB-infected and mock-infected F81 cells at 24, 48, and 72 h postinfection using propidium iodide (PI) staining. We found that MEVB infection was able to arrest the cells in G_1 phase of the cell cycle, which became

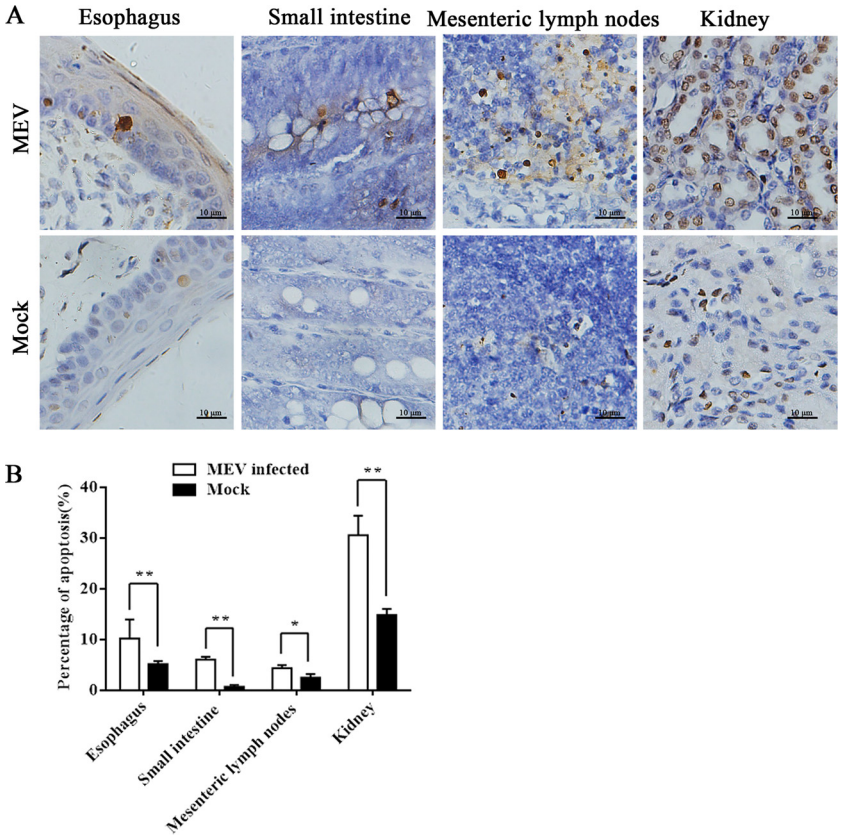

FIG 1 *In situ* TUNEL assay of tissues of minks infected with MEVB. (A) *In situ* TUNEL staining of a single or serially cut tissue sections from the esophagus, small intestine, mesenteric lymph nodes, and kidneys of infected minks, showing an increase of TUNEL-positive cells compared to that in the uninfected group. Images show the macroscopic appearance of the different tissues with TUNEL assay after MEVB infection of the different groups as indicated. (B) Statistical analysis. The histogram summarizes the average percentage of apoptotic cells in the different tissues of infected minks. Data are means ± SEMs from three independent experiments. *, $P < 0.05$; **, $P < 0.01$; these values are statistically significantly different from those of the control group.

more obvious during the course of infection (Fig. 2B). Next, we examined apoptosis in MEVB-infected cells. With the development of infection, the numbers of apoptotic cells were increased significantly at 24 h postinfection in MEVB-infected cells compared with those of mock-infected cells (Fig. 2C). Taken together, these results demonstrated that MEV infection induced apoptosis in F81 cells that was magnified during the course of infection.

MEV NS1 causes cell death. Among the typical cytopathogenic effects of MEV infection are cell rounding and dissociation, which favor the release and spread of progeny viruses. We investigated whether the viral proteins of MEV (VP1, VP2, and NS1) were sufficient to induce cell death using 3-(4,5-dimethyl-2-thiazolyl)-2,5-diphenyl-2H-tetrazolium bromide (MTT) and lactate dehydrogenase (LDH) assays. Compared to that of empty-vector-transfected control cells, NS1-expressing F81 and HEK293T cells had significantly reduced cell viability at 36 h posttransfection, whereas expression of VP1 and VP2 proteins did not affect cell viability (Fig. 3A and B). Over 80% of the F81 and HEK293T cells were transfected by MEV VP1-, VP2-, and NS1-expressing plasmids as detected by immunofluorescence assay (data not shown). Further studies have found that only NS1 protein produced cytolysis of F81 and HEK293T cells, and the greater the toxicity to cells over times (Fig. 3C and D). Z-DEVD-FMK and cisplatin were used as negative and positive controls for apoptosis, respectively, and dimethyl sulfoxide (DMSO) was used as a vehicle control.

In summary, these lines of evidence suggested that only MEV NS1 was sufficient to induce cell death in both F81 and HEK293T cells.

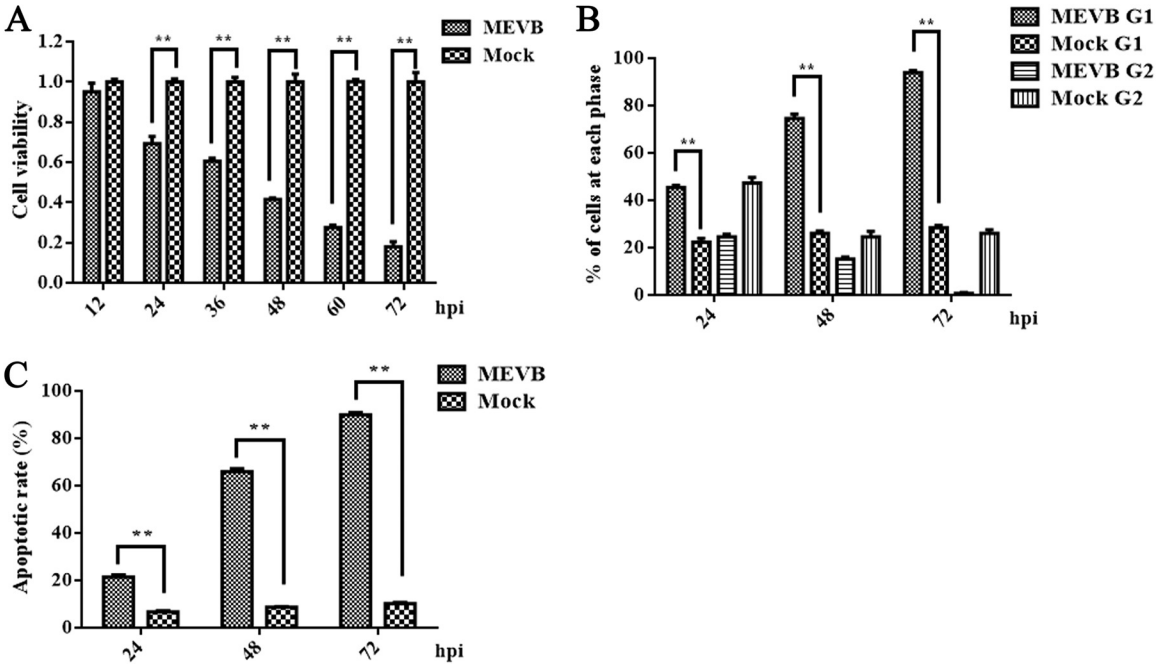

FIG 2 MEV infection induced apoptosis in F81 cells. (A) The cell viability of MEV infected cells was compared to control at different time points postinfection. F81 cells were infected with MEVB at 0.5 MOI and harvested at 12, 24, 36, 48, 60, and 72 h. Cell viability was measured by MTT assay. (B) MEV infection led F81 cells to be arrested at G_1 phase. The DNA contents of F81 cells mock infected or infected with MEVB at an MOI of 0.5 were collected at 24, 48, and 72 h postinfection (hpi), and the cell cycle was analyzed by PI staining and flow cytometry. (C) Apoptosis determination. Cells infected with MEVB at an MOI of 0.5 were stained with annexin V-FITC and PI at different time points postinfection and were analyzed by flow cytometry. Annexin V-positive cells were regarded as apoptotic. Data are means ± SEMs from three independent experiments. *, $P < 0.05$, and **, $P < 0.01$, compared with control groups.

MEV NS1 induces cell cycle arrest and apoptosis but not NS2 and VP1/2. Next, we performed cell cycle analysis of NS1-, VP1-, and VP2-expressing F81 and HEK293T cells at 24, 48, and 72 h posttransfection using PI staining and flow cytometry. Representative cell profiles and histograms of mock-transfected cells and cells expressing different viral proteins are presented in Fig. 4. NS1 was able to arrest most of the cells at G_1 phase among both F81 and HEK293T cells; however, the cell cycle was not affected in *VP1*- or *VP2*-transfected cells (Fig. 4A and B). This assay detected the hypodiploid cell population (sub-G_1 peak), corresponding to the cells undergoing apoptosis (less than 2 N DNA content). We also examined apoptosis following NS1, VP1, and VP2 expression in F81 and HEK293T cells using annexin V and PI staining. Compared to that in the control cells, *NS1*-transfected cells showed a significant increase in apoptosis (Fig. 4C and D). Having confirmed that MEV NS1 induced cell cycle arrest and apoptosis, we asked whether the NS2 protein can induce cycle arrest and apoptosis. We transfected *NS2* into HEK293T cells and analyzed the cells for cell cycle and apoptosis at 24, 48, and 72 h posttransfection. The results showed that NS2 protein neither affected the cell cycle (Fig. 5A) nor induced apoptosis (Fig. 5B).

Taking these results together, we concluded that NS1 is sufficient to induce apoptosis and perturbation of cell cycle in both F81 and HEK293T cells.

MEV NS1 causes mitochondrial damage with ROS accumulation. Disruption of the mitochondrial transmembrane potential is one of the earliest intracellular events that occur following induction of apoptosis. Thus, we examined the impact of NS1 on mitochondrial membrane potential. Our results showed that *NS1*-transfected HEK293T cells had significantly reduced membrane potential starting from 24 h posttransfection compared to those of the mock- and control-transfected cells (Fig. 6A). An increase in the green/red fluorescence intensity was indicative of mitochondrial membrane potential depolarization. We next tested whether NS1-induced apoptosis leads to the opening of mitochondrial transition pores. We analyzed the impact of MEV NS1 on

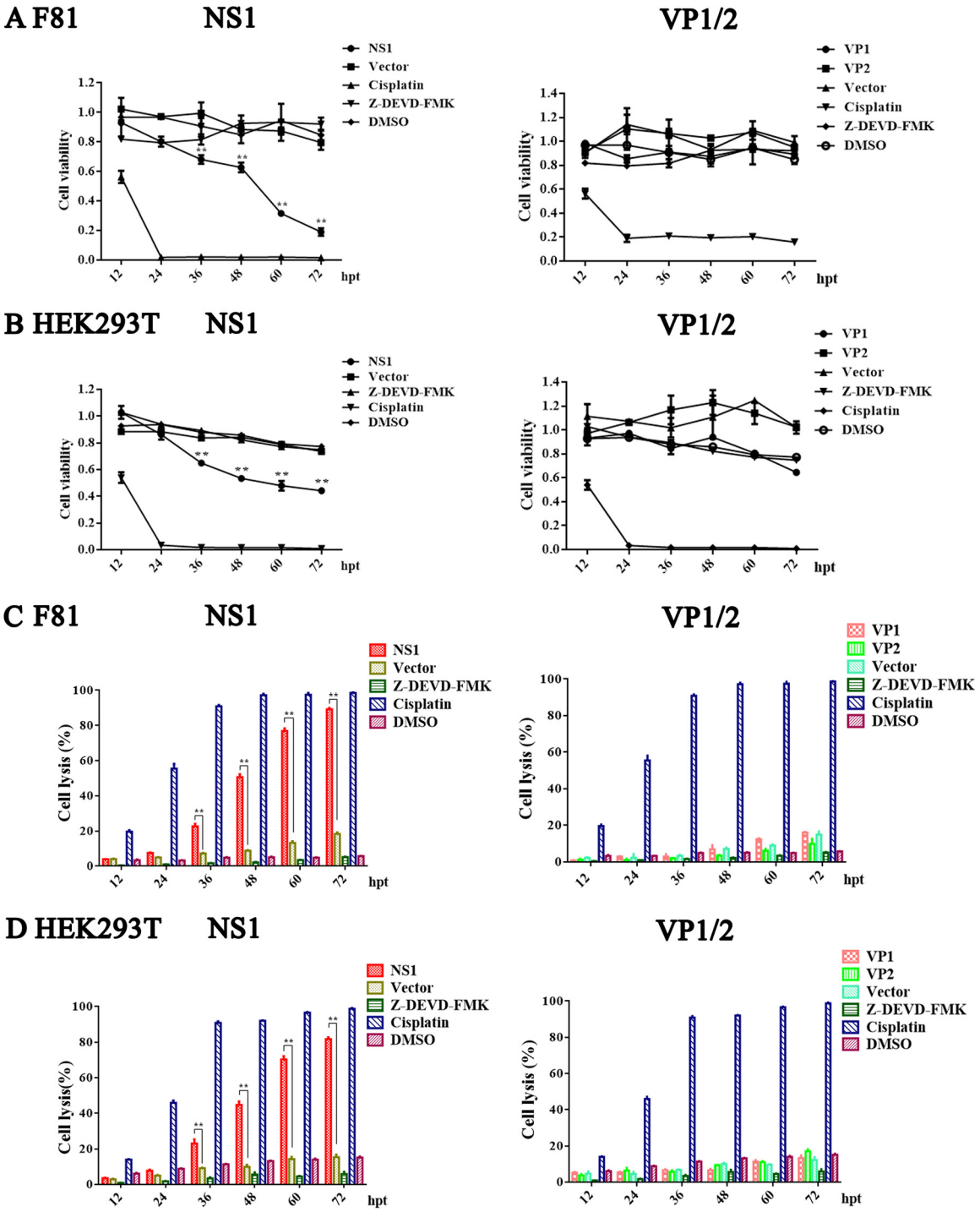

FIG 3 MEV NS1-induced cell death. (A and B) Effects of MEV NS1, VP1, and VP2 on viability of F81 cells (A) and HEK293T cells (B). *NS1*-, *VP1*-, *VP2*- or vector-transfected cells were harvested at the indicated times postinfection for determination of cell viability using the MTT assay. (C and D) The release of LDH was used to assess the cell lysis of transfected F81 cells (C) and HEK293T cells (D) at different time points posttransfection. Z-DEVD-FMK and cisplatin were used as the negative and positive controls for apoptosis, respectively. DMSO was used as a vehicle control. For all assays, data are means ± SEMs, and results from a representative experiment of three independent experiments are shown. *, $P < 0.05$, and **, $P < 0.01$, compared with control groups. hpt, hour posttransfection.

mitochondrial permeability using a mitochondrial permeability transition pore (MPTP) assay. Compared to the vector-transfected cells, *NS1*-transfected cells showed strong induction of apoptosis as shown by the detection of MPTP and hence an increase in mitochondrial permeability (Fig. 6B). ROS plays an important role in the apoptosis

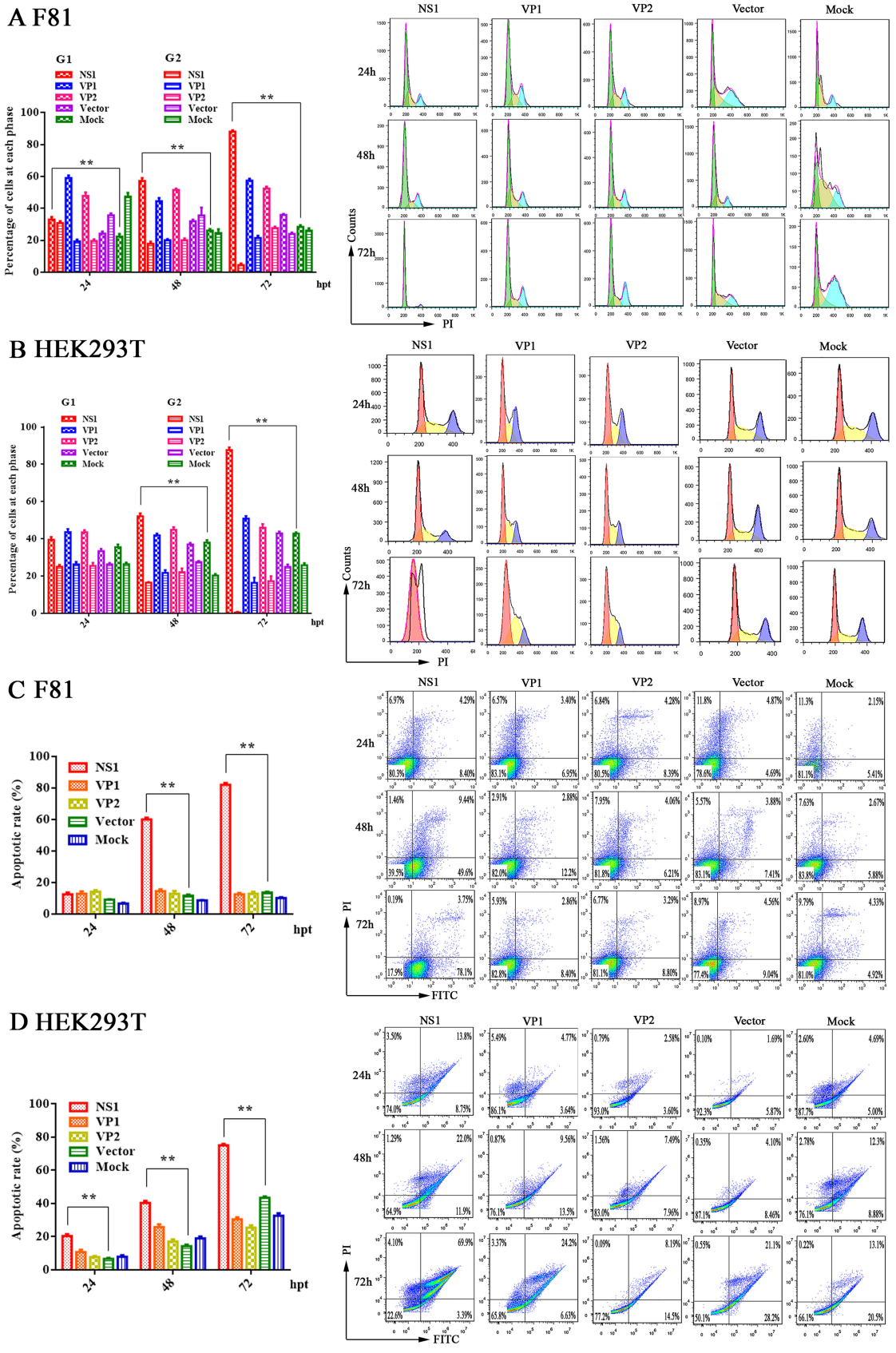

FIG 4 MEV NS1-induced apoptosis. (A and B) F81 (A) and HEK293T cells (B) were transfected with NS1-, VP1-, and VP2-expressing plasmids, as indicated, and subjected to cell cycle analysis by cytometry at 24, 48, and 72 h posttransfection. Empty-vector- and

(Continued on next page)

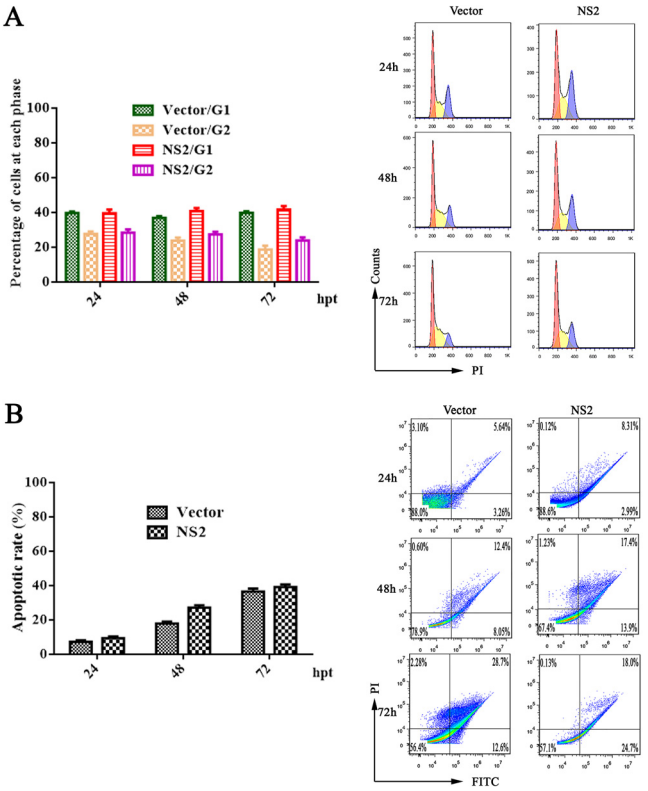

FIG 5 MEV NS2 did not induce apoptosis. HEK293T cells were transfected with NS2-expressing plasmid or empty vector. At 24, 48, and 72 h posttransfection, the cell cycle (A) and apoptotic cells (B) were analyzed by flow cytometry. The histograms show results from representative experiments. The bar charts show the percentages of the cells in G_1 and G_2 phases (A) and the rates of apoptotic cells (B), respectively.

process, activating the mitochondrion-mediated apoptosis pathway. Our observations that MEV NS1 caused mitochondrial membrane depolarization and opening of mitochondrial permeability transition pores prompted us to investigate whether NS1 causes accumulation of ROS and its subsequent release into the cytosol by observation under a spectrophotometer. Compared to that of the mock- and vector-transfected cells, *NS1*-transfected cells had a significant increase in the production of intracellular ROS in a time-dependent manner (Fig. 6C).

Taken together, these data revealed that MEV NS1 was associated with induction of intrinsic apoptosis following mitochondrial damage and triggered ROS accumulation and release into the cytosol.

The intact NS1 protein is essential for inducing apoptosis. The NS1 protein of parvovirus is a multifunctional protein that is composed of the N-terminal replication origin-binding/endonuclease domain (OBD; amino acids [aa] 1 to 337), the helicase activity domain (aa 338 to 556), and the C-terminal transactivation domain (TAD; aa 557 to 668) (Fig. 7A). We thus asked which domain is responsible for inducing apoptosis. To determine this, we constructed plasmids expressing each domain to test their capability to induce apoptosis. Our results showed that the rate of apoptotic cells was not significantly increased when cells were transfected with each domain-expressing plas-

FIG 4 Legend (Continued)
mock-transfected cells were used as negative controls. The histograms show representative cell cycle analyses of *NS1*-, *VP1*-, *VP2*-, empty-vector-, and mock-transfected cells, and the bar charts show percentages of averages and standard error of the mean of the cells in each phase of the cell cycle. (C and D) Apoptosis analysis using annexin V/PI staining. Cells were transfected with the NS1, VP1, VP2, or empty vectors or mock transfected. F81 (C) and HEK293T cells (D) at 24, 48, and 72 h posttransfection were analyzed. The annexin V-positive cells were regarded as apoptotic cells. For all assays, data are representative of results from three independent experiments. *, $P < 0.05$, and **, $P < 0.01$, compared with control groups.

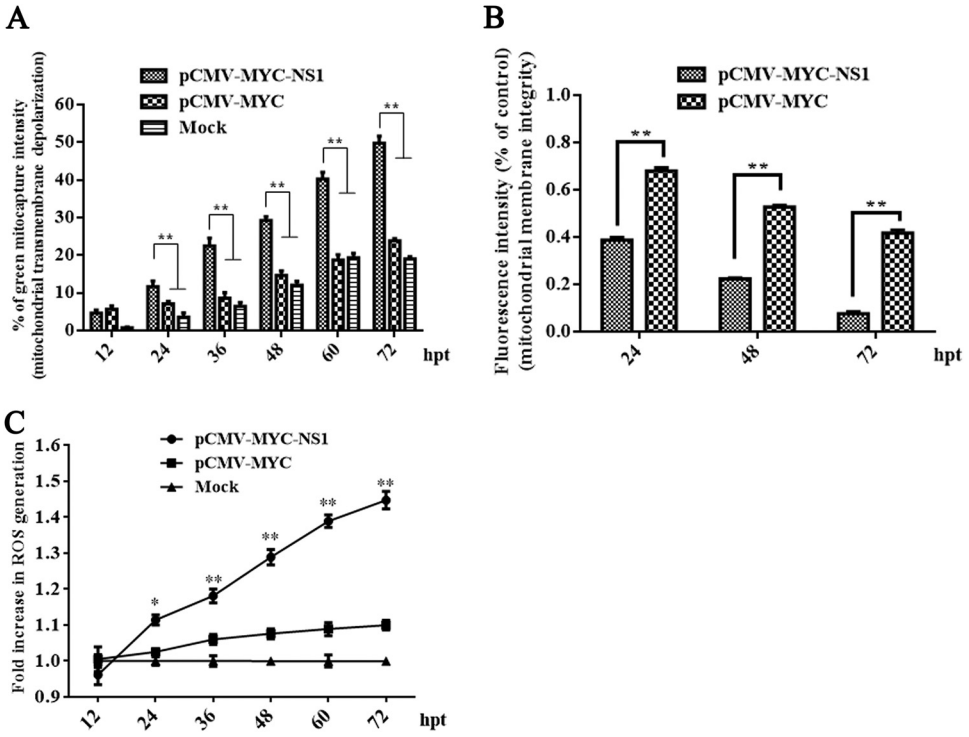

FIG 6 NS1-induced mitochondrial damage with an accumulation of ROS. (A) NS1-induced mitochondrial transmembrane potential depolarization. HEK293T cells were transfected with plasmids as indicated, incubated with MitoCapture reagent, and analyzed by flow cytometry at different time points posttransfection. Vector- and mock-transfected cells were used as negative controls. (B) Loss of mitochondrial membrane integrity in *NS1*-transfected HEK293T cells. Transfected and stained HEK293T cells were captured as overlay histograms. The bar chart presents the significant increase in apoptotic cells with reduced mitochondrial membrane potential after NS1 transfection. (C) Accumulation of ROS in *NS1*-transfected HEK293T cells. *NS1*-transfected HEK293T cells were analyzed at different time points posttransfection, and the production of intracellular ROS was determined fluorometrically. The linear graph presents the increased production of ROS in the *NS1*-transfected cells compared to the mock and vector-transfected cells. Data are expressed as the means ± SEMs and are representative of results from three independent experiments. *, $P < 0.05$, and **, $P < 0.01$, versus the mock control.

mid (Fig. 7C), suggesting that the whole NS1 protein is required to induce apoptosis. We also introduced point mutations into the OBD and helicase domains and deleted the 67 amino acids in the C terminus of the TAD to potentially disrupt the origin binding, helicase, and transactivation activity, respectively (26) (Fig. 7B). As shown in Fig. 7C, point mutations disrupted NS1's capability to induce apoptosis. These results demonstrated that only the full-length MEV NS1 protein has the ability to induce apoptosis and that the origin binding/endonuclease and helicase functions of the NS1 are likely required for the NS1 protein to induce apoptosis.

MEV NS1 initiates apoptosis through activation of caspase-9 and -3 but not caspase-8. We measured the activities of caspase-9 and -3 proteases following NS1 expression in HEK293T cells using the Caspase-Glo 9 and Caspase-Glo 3/7 assays. At 36 h posttransfection, the expression of activated caspase-9 and -3 significantly increased in *NS1*-transfected HEK293T cells compared to mock- or vector-transfected cells (Fig. 8A and B). In order to further prove that NS1 activated caspase-9 and -3, we transfected HEK293T cells with either a pEGFP-NS1 or pEGFP (control) vector. We observed that caspase-9 and -3 were active in pEGFP-NS1-transfected cells but not in pEGFP-transfected cells (Fig. 8C). The activations of caspase-9 and -3 and poly(ADP-ribose) polymerase (PARP) were further confirmed by Western blotting for their specifically cleaved bands. Expressions of cleaved caspase-9 and -3 and PARP were obviously detected at 12 h posttransfection and had increases starting from 36 h posttransfection (Fig. 8D). In contrast, no cleaved caspase-12 was detected, and cleaved caspase-8 was marginally detected at 48 h posttransfection. Thus, we concluded that NS1 expression

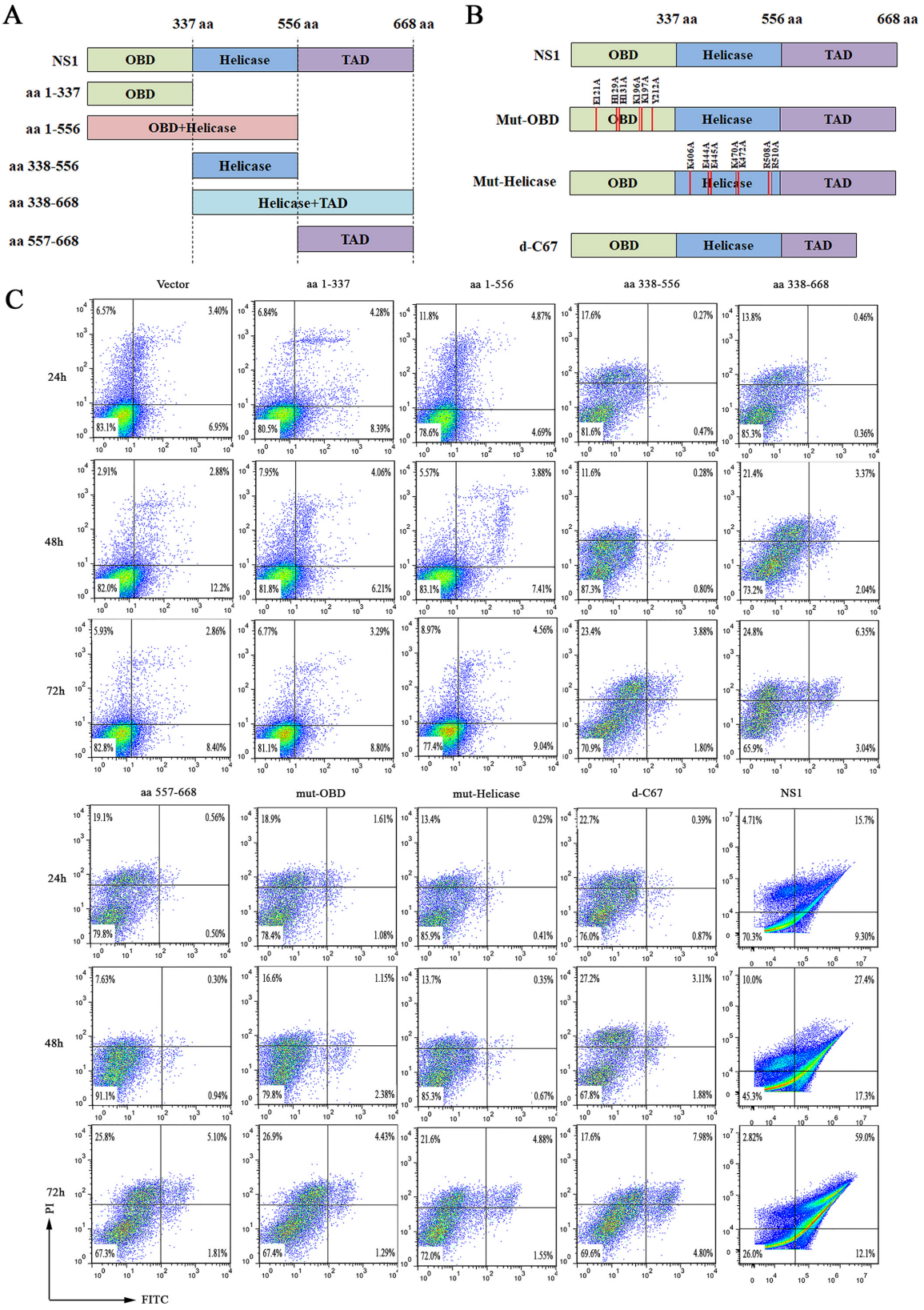

FIG 7 Expression of the full-length MEV NS1 protein was necessary to induce apoptosis. (A and B) Schematic diagram of NS1 mutants. (A) Five NS1 truncated proteins and (B) three NS1 mutants. Positions of each domain are indicated, and the mutated amino acids in the origin-binding (OBD) and helicase domains and the deleted region (C-terminal 67 aa) in the transactivation (TAD) domain are indicated as well. (C) Apoptosis analysis. HEK293T cells were transfected with the five different truncated NS1 proteins and the three NS1 mutants. At 24, 48, and 72 h posttransfection, the cells were analyzed for apoptosis using annexin V/PI staining, followed by flow cytometry.

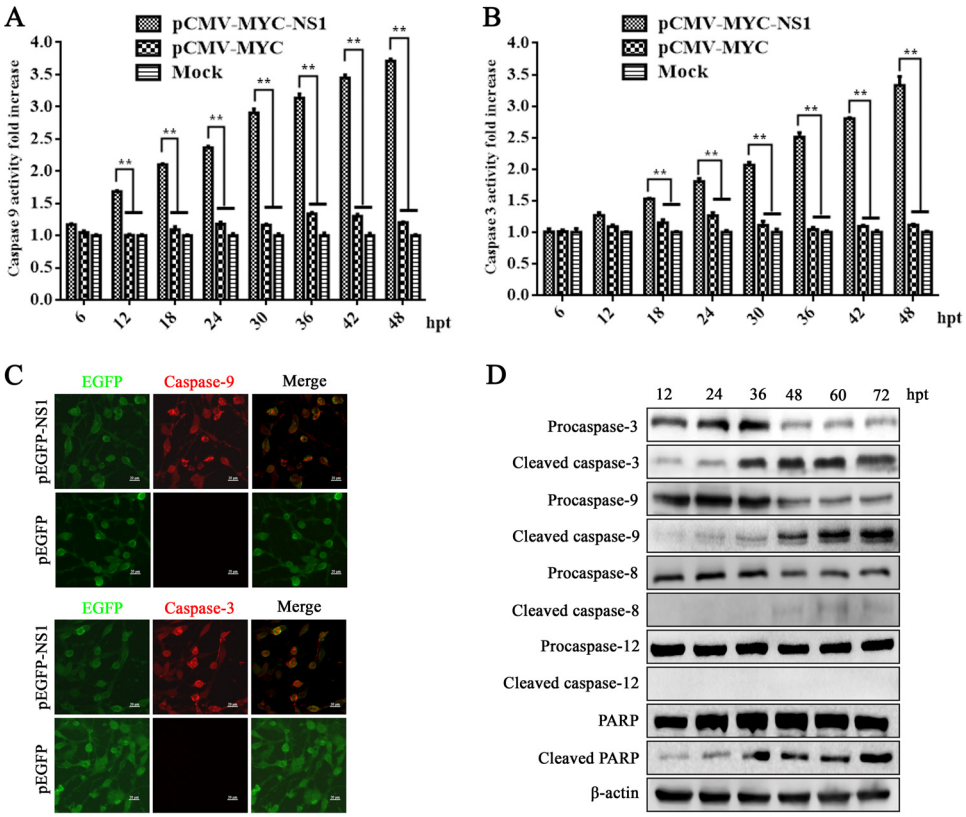

FIG 8 NS1 expression activated caspase-9 and -3. (A and B) Caspase activity in *NS1*-transfected cells. HEK293T cells were transfected with plasmids as indicated. At the indicated time points posttransfection, the caspase-9 and -3 activities of the transfected cells were measured using Caspase-Glo 9 (A) and Caspase-Glo 3/7 (B) luminescent assay kits, respectively. The bar chart presents the means ± SEMs from three independent experiments. *, $P < 0.05$, and **, $P < 0.01$, versus the control group. (C) Caspase-9 and -3 are activated by NS1 expression. HEK293T cells were transfected with pEGFP-NS1 or pEGFP vector. Cells expressing pEGFP-NS1 demonstrated active caspase-9 and -3 with fluorescence in red, while the active caspases were not observed in cells expressing enhanced green fluorescent protein (EGFP) only. (D) Western blotting of pro- and cleaved caspases and PARP. *NS1*- transfected cells were collected at various time points posttransfection and analyzed by Western blotting for expression of caspase-9 and -3, PARP, and their cleaved proteins. β-Actin was probed as a loading control.

mainly activates caspase-9 and -3, but not caspase-8, in NS1-expressing HEK293T cells. These results also suggested that the mitochondrial apoptotic pathway is involved in NS1-induced apoptosis.

MEV NS1 induces apoptosis via a mitochondrion-mediated apoptotic pathway. Next, we aimed to clarify whether the Bcl-2 family proteins function as regulators in the mitochondrial apoptotic pathway (27). We observed the level of the proapoptotic protein (Bax) was upregulated at 24 h after *NS1* transfection, and the expression of the antiapoptotic protein Bcl-2 was slightly downregulated. Additionally, the expression of the activated phosphor-Bcl-2 (Ser 70) was upregulated in *NS1*-transfected HEK293T cells (Fig. 9A). Therefore, NS1 significantly increased the Bax/Bcl-2 ratio, which was critical for the activation of the mitochondrial apoptotic pathway (Fig. 9B). Furthermore, we observed that NS1 protein promoted the translocation of Bax into the mitochondria and the release of cytochrome *c* (Cyt *c*) from the mitochondria into the cytoplasm in HEK293T cells transfected with *NS1*. This confirmed a disruption in mitochondrial function (Fig. 9C). Taken together, these results confirmed that the regulation of Bcl-2 family members and activation of the mitochondrion-mediated apoptotic pathway play a critical role in mediating NS1-caused cell death.

p38 MAPK and p53 pathways play a critical role in NS1-induced apoptosis. In order to identify upstream apoptotic signals induced by NS1, we evaluated the effect of NS1 on the p38 MAPK and p53 signaling pathways. Our results showed that there

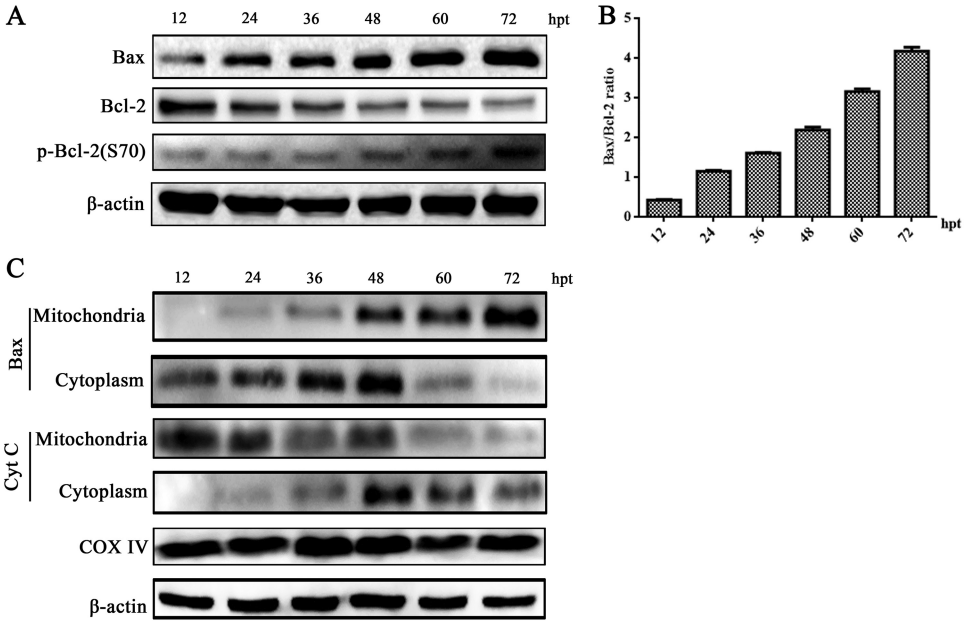

FIG 9 NS1-induced apoptosis was mediated by the activation of mitochondrial pathway. (A and B) Bax and Bcl-2 expression. HEK293T cells were transfected with pCMV-MYC-NS1. At various time points posttransfection as indicated, the cells were analyzed for expression of Bax, Bcl-2, and phosphorylation of Bcl-2 using Western blotting (A). The ratio of Bax/Bcl-2 bands was quantified by densitometry using ImageJ software and plotted (B). (C) Western blot analysis of Bax translocation. HEK293T cells were transfected with pCMV-MYC-NS1. At various time points posttransfection as indicated, the cells were extracted for mitochondria and cytoplasm portions. Bax and Cyt *c* in various compartments were probed by Western blotting. β-Actin and COX-IV were used as endogenous controls for proteins in the cytosolic and mitochondrial fractions, respectively. Representative images from three independent experiments are shown.

was a decrease in the protein levels of p38 MAPK and p53 in a time-dependent manner following transfection. However, our results revealed enhanced expressions of phospho-p53 (Ser 15), phospho-p53 (Ser 20), and phospho-p38 MAPK (Thr 180/Tyr 182) in *NS1*-transfected HEK293T cells, whereas empty vectors cannot activate the p38 MAPK and p53 signal pathways (Fig. 10A). To confirm these results, we used SB203580, a specific inhibitor of p38 MAPK signaling, to inhibit p38 MAPK activation. The downregulation of antiapoptotic Bcl-2 protein expression and the upregulation of expression of proapoptotic Bax were significantly inhibited by SB203580. The downregulation of p53 was also significantly inhibited by SB203580, the specific inhibitor of p38 MAPK. Similarly, the downregulation of antiapoptotic Bcl-2 protein expression and the upregulation of expression of proapoptotic Bax were significantly inhibited by pifithrin-α (a p53 inhibitor) (Fig. 10B).

Together, our results strongly suggested that NS1 induced apoptosis via the intrinsic pathway that is regulated by the activation of p38 MAPK and p53.

DISCUSSION

Apoptosis is a double-edged sword mechanism that is used by the host immune system to combat viral infection and is employed by the virus to induce cytopathogenicity or maximize virus progeny production (28). Apoptosis is mediated by either an intrinsic (mitochondrial) or extrinsic (death receptor) pathway (29). The death receptor-mediated pathway is initiated by activation of tumor necrosis factor receptor superfamily members and followed by recruitment of adaptor molecules and the activation of caspase-8. This triggers the activation of caspase-3 and subsequent apoptosis execution. In contrast, the intrinsic pathway depends on the loss of mitochondrial membrane potential and the increase of membrane permeability, leading to the release of toxic proteins that activate and initiate the caspase cascade (30).

Parvovirus NS1 protein mediates the cytotoxic and pathogenic effects of parvovirus

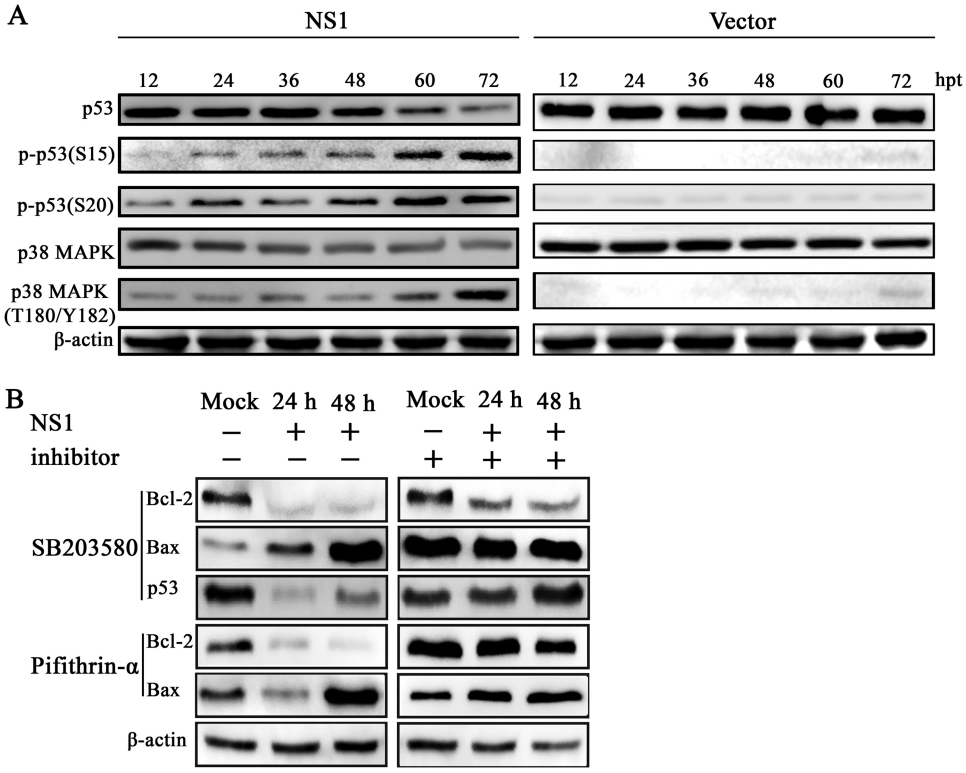

FIG 10 NS1 activated the p38 MAPK and p53 signaling pathways. (A) Analysis of p38 MAPK and p53 expression. HEK293T cells were transfected with pCMV-MYC-NS1 (left) or pCMV-MYC (right). At various time points posttransfection as indicated, the cells were analyzed for levels of total p38 MAPK and p53 and their phosphorylated forms by Western blotting. (B) Inhibition of p38 MAPK and p53 activation altered the expression of Bcl-2 and Bax. HEK293T cells were pretreated with a 20 μM concentration of the p38 MAPK inhibitor SB203580 or p53 inhibitor pifithrin-α for 18 h, followed by transfection with *NS1*. At 24 and 48 h posttransfection, the cells were subjected to Western blotting using antibodies against Bcl-2, Bax, and p53. β-Actin was probed as a loading control.

infection in permissive cells (31). Accumulating evidence demonstrates the ability of parvovirus and its NS1 protein to induce apoptosis (14, 16, 32). Therefore, we aimed to investigate the exact mechanism for MEV and its NS1 in MEV infection-caused apoptosis. Our present study revealed that MEV induces apoptosis in the infected esophagus, small intestine, mesenteric lymph nodes, and kidneys *in vivo*, as well as in F81 cells. However, no apoptotic cells were found in the tongue tissue. Since the tissue of the surface of the tongue is composed of complex flat epithelial cells, which do not divide vigorously, and parvovirus replicates in proliferating cells (33), the tongue tissue was not infected. F81 cells are feline kidney cells and are permissive for MEV infection, which drove our attention to test apoptosis in the kidney. We found that apoptosis in the kidney is more significant than that in other tissues. Thus, we believe that apoptosis is related to virus infection. These results are consistent with the clinical symptoms of the infected mink, such as severe diarrhea and feces containing sloughed-off gray intestinal mucosal cells. Meanwhile, our results confirmed that MEV NS1 expression in F81 and HEK293T cells appeared to cause nuclear condensation and fragmentation as well as annexin V-positive staining, which are the typical characteristics of apoptosis. Furthermore, we found that full-length MEV NS1 induced apoptosis through activating p38 MAPK and p53 signaling and ultimately the mitochondrial pathway.

Our results demonstrated that the ratio of the proapoptotic Bax and antiapoptotic Bcl-2 was increased in NS1-transfected HEK293T cells, which is in agreement with previous reports (11, 20, 34). Additionally, similar to the NS1 proteins of other parvoviruses (such as CPV, H-1PV, MVC, and B19), MEV NS1 caused mitochondrial depolarization and increased mitochondrial permeability, which were evidenced by the efflux of Cyt *c* and the subsequent upregulation of caspase-9 and -3 (30). On the other hand,

MEV NS1 did not change the activity of caspase-8, implying that the extrinsic apoptotic pathway is not involved in NS1-induced apoptosis (11, 21, 35).

Parvovirus NS1 protein is known for its ability to cause cell cycle arrest at various phases depending on the virus and the host cell type (16, 36). Following MEV NS1 transfection, we analyzed the cell cycle progression using flow cytometry. Similar to other parvoviral NS1 proteins, MEV NS1 arrested most of the transfected cells at the G_1 phase (20, 23, 35). The G_1-phase cell cycle arrest could be attributed to the upregulation of cyclin kinase inhibitors (CKIs), such as p21 and p27 (37, 38).

ROS are mainly generated in the mitochondria, and their excessive production leads to oxidative stress. Furthermore, excessive ROS production also triggers the release of Cyt *c* from the mitochondria (39). The release of ROS into the cytosol possibly induces cellular apoptosis (11, 40). In this study, MEV NS1 significantly increased the accumulation of ROS in *NS1*-transfected cells. However, the exact mechanism underlying MEV NS1-mediated ROS accumulation remains unclear. It could be attributed to the deregulation of the mitochondrial ROS metabolic enzymes (41). H-1PV NS1 resulted in the accumulation of ROS in HEK293 and HeLa cells, which subsequently causes H-1PV-mediated cytotoxicity (11). Similarly, oxidative stress is induced by other viral proteins, such as the Vpr protein of HIV (42), hepatitis C virus core protein (43), and the NS1 protein of the avian influenza virus H9N2 (44). Nevertheless, future studies are required to identify the mechanism underlying MEV NS1-mediated ROS accumulation.

p53, a tumor suppressor protein, is a transcription factor with pivotal roles in the regulation of the cell stress response, including the regulation of Bax and Bcl-2 expression (45). Previous research demonstrated the activation of p53 in MVM, PPV, and B19-induced apoptosis (17, 46, 47). In *NS1*-transfected cells, we demonstrated that NS1 caused p53 phosphorylation. Interestingly, pretreatment of the *NS1*-transfected cells with a p53 inhibitor, pifithrin-α, altered the expression of Bcl-2 and Bax proteins. The p38 MAPK, belonging to the mitogen-activated protein kinase signaling pathway, has been implicated in the immune and inflammatory responses via the regulation of several signal transduction pathways, including apoptosis (48, 49). Our results showed that p38 MAPK was phosphorylated at threonine 180 and tyrosine 182, which activates p53 via phosphorylation at serines 15 and 20 (50). On the other hand, the inhibition of p38 MAPK phosphorylation suppressed p53 activation, affecting the expression levels of Bax and Bcl-2. Although NS1 expression was able to transactivate the promoter of p38 MAPK ~2-fold (data not shown), the level of p38 MAPK protein was decreased over the time of transfection (Fig. 10A). Therefore, we believe that NS1 targets activation of p38 MAPK through transactivating expression of other factors upstream of p38 MAPK, which merits further investigation. Activated p38 MAPK directly phosphorylates p53, which induces a cascade of apoptotic death signaling in NS1-expressing cells (Fig. 11).

The fact that intact NS1 of MEV and potentially all the functions of DNA binding, endonuclease, and transactivation are necessary to induce apoptosis strongly indicates that the transactivation function of MEV NS1 in the expression of p38 MAPK and host proteins that are upstream of p38 MAPK requires NS1 binding to their promoter. This process may require oligomerization of NS1 as reported for other parvoviral NS1 proteins (51, 52). In future studies, we will identify the factors upstream of p38 MAPK that are likely transactivated by MEV NS1.

MATERIALS AND METHODS

Ethics statement. All experimental protocols were approved by the Ethical Committee of the Institute of Special Animal and Plant Sciences, Chinese Academy of Agricultural Sciences. The collection of specimens in this work strictly complied with the approved guidelines and regulations of the Animal Care and Use Committee.

Virus and cell lines. HEK293T cells and feline kidney cells (F81 cells) were purchased from the American Type Culture Collection and were cultured in Dulbecco's modified Eagle medium (DMEM; HyClone, Logan, UT) supplemented with 8% heat-inactivated fetal bovine serum (BI, Kibbutz Beit Haemek, Israel) in 5% CO_2 at 37°C. Strain MEVB was obtained from the Institute of Special Animal and Plant Sciences, Chinese Academy of Agricultural Sciences. MEVB was propagated in F81 cells cultured at

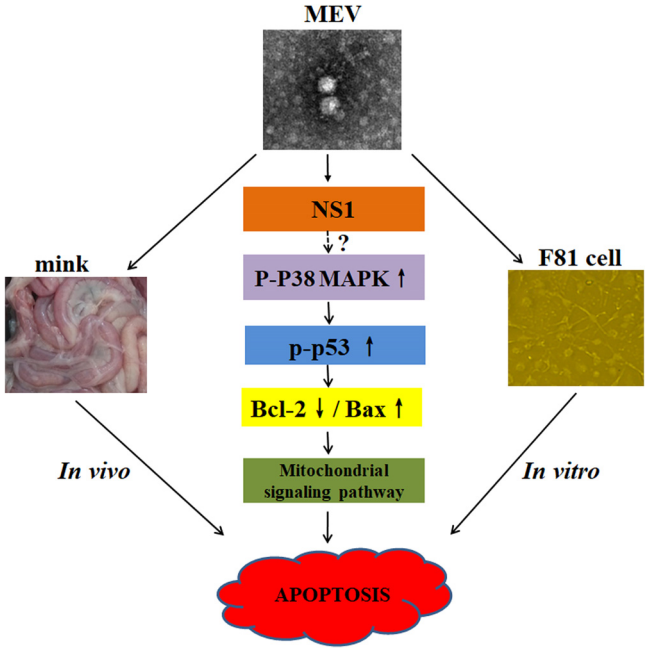

FIG 11 A proposed model for MEV NS1-induced mitochondrion-mediated apoptosis. MEV infection induces apoptosis both *in vivo* and *in vitro*. The full-length MEV NS1 protein induces apoptosis through activating the mitochondrial pathway through indirectly activating p38 MAPK by phosphorylation at threonine 180 and tyrosine 182. The activated p38 MAPK then directly activates p53 via phosphorylation at serines 15 and 20, thereby decreasing Bcl-2 expression and increaing Bax expression, which motivates mitochondrial damage and progression of apoptosis.

37°C. At 72 h postinfection, the cultures were frozen and thawed 3 times and stored at −80°C. F81 cells were added to 6-well plates and concurrently infected with MEVB (multiplicity of infection [MOI] = 0.5). The infected cells were harvested at different times postinfection to carry out the study. The uninfected F81 cells acted as a control.

Antibodies used. The following primary antibodies were used: anti-β-actin (60008), anti-glyceraldehyde-3-phosphate dehydrogenase (anti-GAPDH; 60004), anti-COX-IV (11242), anti-caspase-3 (19677), anti-caspase-9 (66169), anti-caspase-8 (13423), anti-cytochrome *c* (10993), and anti-Bcl-2 (12789) from Proteintech (Chicago, IL); anti-MYC (TA150121) from ORIGENE (Rockville, MD); and anti-Bax (5023), anti-PARP (9532), anti-cleaved PARP (Asp 214) (5625), anti-cleaved caspase-3 (Asp 175) (9664), anti-cleaved caspase-9 (Asp 330) (52873), anti-cleaved caspase-8 (Asp 387) (8592), anti-p53 (2524), anti-phospho-p53 (Ser 15) (9286), anti-phospho-p53 (Ser 20) (9287), anti-phospho-Bcl-2 (Ser 70) (2827), anti-p38 MAPK (8690), and anti-phospho-p38 MAPK (Thr 180/Tyr 182) (4511) from Cell Signaling Technology (Danvers, MA). Anti-MEV NS1 and VP mouse monoclonal antibodies and anti-MEV NS2 mouse polyclonal antibody were prepared in our laboratory.

Secondary antibodies were as follows: horseradish peroxidase (HRP)-labeled goat anti-mouse (SA00001-1) and HRP-labeled goat anti-rabbit (SA00001-2) from Proteintech (Chicago, IL) and goat anti-mouse IgG (H+L) Texas Red (BS10002) and goat anti-rabbit IgG (H+L) Texas Red (BS10003) from Bioworld (St. Louis Park, MN).

DNA constructs. For pCMV-MYC-NS1, pCMV-MYC-NS1$^{1\text{-}337}$, pCMV-MYC-NS1$^{1\text{-}556}$, pCMV-MYC-NS1$^{338\text{-}556}$, pCMV-MYC-NS1$^{338\text{-}668}$, pCMV-MYC-NS1$^{557\text{-}668}$, and pEGFP-NS1, DNA samples were extracted from MEV-infected F81 cells and stored as previously described (53). The primers were designed based on a sequence deposited in GenBank under accession number FJ592174 (Table 1). All or a part of the NS1 ORF was amplified, purified, and cloned into pCMV-MYC or pEGFP-C1 (pEGFP) vector between the restriction sites PstI/XhoI and BamHI, resulting in generation of the full-length or truncated NS1 expression plasmids as listed above.

For pCMV-MYC-VP2, pCMV-MYC was used to clone the *VP2* ORF between the restriction sites XhoI and BamHI, as described above.

For pCMV-Flag-VP1 and pCDNA3.1(+)-Flag-NS2, MEVB *VP1* (nucleotides [nt] 2168 to 2199 and 2269 to 4423) and *NS2* (nt 155 to 415 and 1887 to 2124) genes were synthesized from Genecreate Corporation (Wuhan, China). The genes were subcloned into the pCMV-Flag and pCDNA3.1(+)-Flag vectors using restriction enzymes BamHI and XhoI, yielding the plasmids pCMV-Flag-VP1 and pCDNA3.1(+)-Flag-NS2.

For pCMV-MYC-NS1^{muts}, the *NS1* gene sequence was mutated using PCR-based site-directed mutagenesis or a two-step PCR method to generate pCMV-MYC-NS1$^{mut\text{-}OBD}$, pCMV-MYC-NS1$^{mut\text{-}Helicase}$, and pCMV-MYC-NS1$^{d\text{-}C67}$ (Fig. 7B).

All constructs were sequenced at Comate Bioscience Co., Ltd. (Changchun, China).

DNA transfection. At 60 to 70% confluence, cells were transfected with constructs and parental vector with X-tremeGENE HP DNA transfection reagent (Roche, Philadelphia, PA), using the manufac-

TABLE 1 Primer sequences used for amplification of MEV genes

Primer name	Sequence (5′–3′)	Positions[a]
MEV *NS1*-F/R	CGC **CTG CAG** ATG TCT GGC AAC CAG TAT A CGG **GGA TCC** TTA ATC CAA GTC GTC TCGAA	155–2161
MEV *VP2*-F/R	**GGA TCC** ACC ATG AGT GAT GGA G CCG **CTC GAG** TCA ATA TAA TTT TCT AGG	2669–4423
NS1 1-337 F/R	AA**G GAT CC**G CCA CCA TGT CTG GCA ACC GGA CGC **GTC GAC** TTA TCT TGC TAA AGT CA	155–1165
NS1 1-556 F/R	AA**G GAT CC**G CCA CCA TGT CTG GCA ACC CAC GC**G TCG AC**T TAT CCC CAA TGA TGT GT	155–1823
NS1 338-556 F/R	**GGA TCC** GCC ACC ATG ACA AAA ACA GCA TTT CAC GC**G TCG AC**T TAT CCC CAA TGA TGT GT	1166–1823
NS1 338-668 F/R	**GGA TCC** GCC ACC ATG ACA AAA ACA GCA TTT GCC GC**G TCG AC**T TAA TCC AAG TCG TCT CG	1166–2161
NS1 557-668 F/R	**GGA TCC** GCC ACC ATG AAA GTA CCA GAA TGG G GCC GC**G TCG AC**T TAA TCC AAG TCG TCT CG	1823–2161

[a]Primer positions refer to the nucleotide sequence of strain MEVB (GenBank accession number FJ592174). Boldface and underlined sequences represent restriction sites.

turer's standard protocol. Untransfected cells and the parental vector served as mock and vector controls, respectively. For pretreatment, cisplatin (apoptosis activator; S1166; Selleckchem, Houston, TX), Z-DEVD-FMK (caspase-3 inhibitor; S7312; Selleckchem), SB203580 (p38 MAPK inhibitor; S1076; Selleckchem), and pifithrin-α (p53 inhibitor; S2929; Selleckchem) were used at 20 μM for *in vitro* experiments. Control groups were treated with DMSO at the same volume.

***In vivo* experiments.** Fifteen 10-week-old healthy minks were supplied by Changbai Mountain Wildlife Resource Key Field Scientific Experimental Station of the Ministry of Agriculture and Rural Affairs PRC. All minks were negative for MEV and neutralizing antibody of MEV (titer $<$ 1:2). Ten minks were orally inoculated with 10 ml of medium containing $1 \times 10^{5.5}$ 50% tissue culture infective doses ($TCID_{50}$)/ml of MEVB, and minks in the control group ($n = 5$) were administered with the same dose of medium without virus. After inoculation, the minks were observed and observations were recorded three times daily for 14 days for clinical symptoms and gastrointestinal clinical signs; minks were humanely euthanized after the appearance of severe diarrhea or after becoming moribund, in accordance with the guidelines of the Ethical Committee of the Institute. Tissue samples of esophagus, small intestine, mesenteric lymph nodes, and kidney were fixed in 10% neutral buffered formalin for 24 h and embedded in paraffin wax.

***In situ* detection of apoptosis.** For *in situ* detection of apoptosis, the TUNEL assay was performed according to the method of Chen et al. (54), with minor modifications. Tissue sections were dewaxed, rehydrated, and treated for quenching of endogenous peroxidase activity as described above. The TUNEL analysis was carried out in sections for the histological detection of apoptotic cells using a TUNEL apoptosis detection kit (KGA702; KeyGEN, Nanjing, China) according to the manufacturer's instructions. The samples of the mock group were used as controls.

Fluorescence microscopy. Transfected cells were analyzed for the expression of NS1 protein by immunofluorescence. Briefly, at 48 h posttransfection, cells were washed three times with ice-cold phosphate-buffered saline (PBS) and fixed with 4% paraformaldehyde (PFA), followed by permeabilization with 0.3% Triton X-100. Cells were incubated with different primary antibodies and then incubated with anti-rabbit or mouse Texas Red-labeled secondary antibody for 1 h. Images were taken using an EVOS FL cell imaging system (Thermo Fisher Scientific, Waltham, MA).

Cell viability assessment. (i) MTT assay. Cell viability was detected by MTT assay (KGA311; Keygen, Nanjing, China) as previously described (55). Briefly, cells were seeded in 96-well plates and concurrently infected with MEVB (MOI = 0.5) or transfected with different vectors after 12 h of culture. Next, 50 μl of MTT working solution was added into each well and the plate was incubated for another 4 h (the MTT buffer dilution was 1:4). Finally, the formazan crystals were dissolved by DMSO and the absorbance was measured by a microplate spectrophotometer (Biotek, Winooski, VT) at 550 nm. Data are presented as percentages of the control wells.

(ii) LDH assay. Cells were seeded into 96-well plates in 100 μl of culture medium. After 12 h, the cells were infected or transfected of MEVB or different vectors. The release of LDH was used to assess cell death using a cytotoxic assay kit (C0016; Beyotime, Shanghai, China). Briefly, the assay buffer was prepared and added to the transfected cells according to the manufacturer's protocol. The optical density (OD) was measured at 490 nm with a spectrophotometer. The percentage of LDH released is the LDH activity in the medium divided by the total LDH activity multiplied by 100.

Flow cytometry analysis. (i) Cell cycle analysis. The DNA content of cells was determined by flow cytometric analysis at 24, 48, and 72 h posttransfection or postinfection. The cells were harvested by 0.25% trypsin, washed, fixed with 70% ice-cold ethanol (added dropwise), and stored at −4°C overnight. Next, the cells were centrifuged at 500 $\times$ *g* for 5 min and washed with PBS. The centrifugation pellet was then resuspended in 500 μl of resuspension buffer (20 μg/ml of RNase A and 180 μg/ml of PI) for 60 min in the dark. The cell cycle was analyzed by flow cytometry, and data were processed with CellQuest (BD Biosciences) software.

(ii) Annexin V-FITC/PI assay. An annexin V-fluorescein isothiocyanate (FITC) apoptosis detection kit (APOAF; Sigma-Aldrich, St. Louis, MO) was used to detect the percentage of apoptotic cells, according to

the manufacturer's instructions. Cells were harvested at 24, 48, and 72 h after infection with MEVB or after transfection of plasmids, followed by digestion with trypsin without EDTA, washing with ice-cold PBS, and centrifugation. The pellet was gently resuspended in 500 μl of binding buffer, 5 μl of annexin V-FITC, and 10 μl of PI. After incubation at room temperature for 20 min, the samples were analyzed on a flow cytometer (Becton, Dickinson, San Jose, CA) within 60 min.

Detection of mitochondrial membrane potential. The mitochondrial membrane potential was detected using a MitoCapture mitochondrial apoptosis detection kit (K250-100; Biovision, San Francisco, CA). MitoCapture accumulates in the mitochondrial matrix, forming red fluorescence. Upon apoptosis, the altered mitochondrial membrane potential prevents MitoCapture from aggregating in the mitochondrial matrix and the dye becomes dispersed throughout the cell, leading to the detection of green fluorescent MitoCapture monomers. *NS1*-transfected cells were harvested at different time points, resuspended in 1 ml of MitoCapture solution, and incubated for 1 h at 37°C. Next, the cells were centrifuged for 3 min at 13,000 $\times$ *g*, and the pellet was resuspended in 1 ml of incubation buffer (prewarmed at 37°C). Subsequently, the samples were analyzed by flow cytometry within 60 min.

Mitochondrial permeability assay. Mitochondrial permeability was examined with a mitochondrial permeability transition pore assay kit (K239-100; Biovision, San Francisco, CA). Transfected cells were incubated with 1 ml of MPTP wash buffer. Then the samples were divided into four treatment groups: sample 1 was not treated, sample 2 was treated with MPTP staining dye, sample 3 was treated with MPTP staining dye and $CoCl_2$, and sample 4 was treated with MPTP staining dye, $CoCl_2$, and ionomycin. All aliquots were incubated for 30 min at 37°C in the dark. Following incubation, the cells were centrifuged at 1,000 $\times$ *g* for 8 min, resuspended in 1 ml of MPTP wash buffer, and analyzed by flow cytometry within 60 min.

Detection of ROS. The estimation of intracellular ROS was performed by using a fluorometric intracellular ROS kit (MAK143; Sigma-Aldrich, St. Louis, MO), according to the manufacturer's protocol. In brief, ROS reaction mix assay stain was added to the treatment and control wells, and the cells were then incubated for 2 h at 37°C in 5% CO_2. After incubation, samples were analyzed on a spectrophotometer at 540-nm excitation and 570-nm emission wavelengths.

Assessment of caspase activities. Caspase-9 and -3 activities were measured using the Caspase-Glo 9 and Caspase-Glo 3/7 assays (G8211 and G8091, respectively; Promega, Madison, WI). Cells were plated in a 96-well cell culture plate, followed by transfection or infection. The cells were then evaluated for caspase-9 and -3 activities according to the manufacturer's protocol on Synergy H1 (BioTek, Winooski, VT). Meanwhile, a 24-well cell culture plate was overlaid with caspase-9 or -3 antibodies in 50 μl of 5% bovine serum and incubated for 1 h. Cells were washed three times with wash buffer and then incubated with goat anti-mouse/rabbit IgG (H+L) Texas Red (1:200) for 1 h at room temperature. The caspase-9 and -3 activities were assayed by immunofluorescence.

Cytosolic fractionation. To detect the release of mitochondrial proteins, cell pellets were washed with cold PBS. Mitochondria were isolated using a cell mitochondrion isolation kit (C3601; Beyotime, Shanghai, China). Briefly, cells were resuspended in a lysis buffer and passed 10 times through a 26-gauge needle. The cell lysates were centrifuged, and both the supernatants and precipitates were collected. The protein concentrations of the cytosolic (supernatant) and mitochondrial (pellet) fractions were determined with a bicinchoninic acid (BCA) protein assay kit (23225; Thermo Fisher Scientific, Waltham, MA). The protein samples were separated by SDS-PAGE for Western blotting.

Western blotting. Transfected cells were trypsinized and washed with ice-cold PBS. Following centrifugation, proteins were extracted by incubation with lysis buffer (NP-40 containing 1% phenylmethylsulfonyl fluoride [PMSF]) from the cell pellets for 30 min at 4°C. After centrifugation (at 13,000 rpm for 20 min), the protein concentration was determined in the supernatants by a BCA protein assay kit, using the manufacturer's instructions. A total of 30 μg of proteins was separated by 12 to 15% SDS-PAGE and transferred onto a polyvinylidene difluoride (PVDF) membrane (GE Healthcare, Buckinghamshire, UK). After blocking in 5% skim milk for 2 h, the membrane was incubated with primary antibodies overnight at 4°C and washed, followed by incubation with HRP-conjugated secondary antibody for 1 h at room temperature. Signals were developed using an ECL detection kit (34577; Thermo Fisher Scientific, Waltham, MA). The intensity of the bands was analyzed using the ImageJ image processing program (53).

Statistical analysis. The statistical differences between the MEVB-infected, NS1-transfected, and control or mock groups were examined by a Student *t* test. Results are expressed as averages plus or minus the standard errors of the means and are representative of those from three independent experiments. Statistical analyses were carried out using GraphPad Prism 6 (GraphPad Software; San Diego, CA). A *P* value of <0.05 was considered to be statistically significant.

ACKNOWLEDGMENTS

This study was supported by the National Natural Science Foundation of China (no. 31602056) and the Jilin Province Scientific and Technological Program (no. 20160520034JH).

The funders had no role in study design, data collection and interpretation, or the decision to submit the work for publication.

We declare that we have no competing interests.

REFERENCES

1. Trump BF, Berezesky IK, Chang SH, Phelps PC. 1997. The pathways of cell death: oncosis, apoptosis, and necrosis. Toxicol Pathol 25:82–88. https://doi.org/10.1177/019262339702500116.
2. Giorgi C, Wieckowski MR, Pandolfi PP, Pinton P. 2011. Mitochondria associated membranes (MAMs) as critical hubs for apoptosis. Commun Integr Biol 4:334–335. https://doi.org/10.4161/cib.4.3.15021.
3. Green DR, Llambi F. 2015. Cell death signaling. Cold Spring Harb Perspect Biol 7:a006080. https://doi.org/10.1101/cshperspect.a006080.
4. Lee S, Hirohama M, Noguchi M, Nagata K, Kawaguchi A. 2018. Influenza A virus infection triggers pyroptosis and apoptosis of respiratory epithelial cells through the type I interferon signaling pathway in a mutually exclusive manner. J Virol 92:e00396-18. https://doi.org/10.1128/JVI.00396-18.
5. Zan J, Liu J, Zhou JW, Wang HL, Mo KK, Yan Y, Xu YB, Liao M, Su S, Hu RL, Zhou JY. 2016. Rabies virus matrix protein induces apoptosis by targeting mitochondria. Exp Cell Res 347:83–94. https://doi.org/10.1016/j.yexcr.2016.07.008.
6. Ding L, Zhao X, Huang Y, Du Q, Dong F, Zhang H, Song X, Zhang W, Tong D. 2013. Regulation of ROS in transmissible gastroenteritis virus-activated apoptotic signaling. Biochem Biophys Res Commun 442:33–37. https://doi.org/10.1016/j.bbrc.2013.10.164.
7. Lee SM, Kleiboeker SB. 2007. Porcine reproductive and respiratory syndrome virus induces apoptosis through a mitochondria-mediated pathway. Virology 365:419–434. https://doi.org/10.1016/j.virol.2007.04.001.
8. Wang J, Zhao H, Cheng Y, Yi L, Cheng S. 2013. Genome sequence of mink enteritis virus strain SD 12/01, isolated from a mink with severe diarrhea in China. Genome Announc 1:e00306-13. https://doi.org/10.1128/genomeA.00306-13.
9. Lin P, Wang H, Cheng Y, Song S, Sun Y, Zhang M, Guo L, Yi L, Tong M, Cao Z, Li S, Cheng S, Wang J. 2018. Loop-mediated isothermal amplification-single nucleotide polymorphism analysis for detection and differentiation of wild-type and vaccine strains of mink enteritis virus. Sci Rep 8:8393. https://doi.org/10.1038/s41598-018-26717-6.
10. Wang J, Cheng S, Yi L, Cheng Y, Yang S, Xu H, Li Z, Shi X, Wu H, Yan X. 2013. Detection of mink enteritis virus by loop-mediated isothermal amplification (LAMP). J Virol Methods 187:401–405. https://doi.org/10.1016/j.jviromet.2012.11.012.
11. Hristov G, Kramer M, Li J, El-Andaloussi N, Mora R, Daeffler L, Zentgraf H, Rommelaere J, Marchini A. 2010. Through its nonstructural protein NS1, parvovirus H-1 induces apoptosis via accumulation of reactive oxygen species. J Virol 84:5909–5922. https://doi.org/10.1128/JVI.01797-09.
12. Nuesch JP, Rommelaere J. 2006. NS1 interaction with CKII alpha: novel protein complex mediating parvovirus-induced cytotoxicity. J Virol 80:4729–4739. https://doi.org/10.1128/JVI.80.10.4729-4739.2006.
13. Bauder B, Suchy A, Gabler C, Weissenbock H. 2000. Apoptosis in feline panleukopenia and canine parvovirus enteritis. J Vet Med B Infect Dis Vet Public Health 47:775–784. https://doi.org/10.1046/j.1439-0450.2000.00411.x.
14. Zhang H, Huang Y, Du Q, Luo X, Zhang L, Zhao X, Tong D. 2015. Porcine parvovirus infection induces apoptosis in PK-15 cells through activation of p53 and mitochondria-mediated pathway. Biochem Biophys Res Commun 456:649–655. https://doi.org/10.1016/j.bbrc.2014.12.011.
15. Ohshima T, Iwama M, Ueno Y, Sugiyama F, Nakajima T, Fukamizu A, Yagami K. 1998. Induction of apoptosis in vitro and in vivo by H-1 parvovirus infection. J Gen Virol 79:3067–3071. https://doi.org/10.1099/0022-1317-79-12-3067.
16. Doley J, Singh LV, Kumar GR, Sahoo AP, Saxena L, Chaturvedi U, Saxena S, Kumar R, Singh PK, Rajmani RS, Santra L, Palia SK, Tiwari S, Harish DR, Kumar A, Desai GS, Gupta S, Gupta SK, Tiwari AK. 2014. Canine parvovirus type 2a (CPV-2a)-induced apoptosis in MDCK involves both extrinsic and intrinsic pathways. Appl Biochem Biotechnol 172:497–508. https://doi.org/10.1007/s12010-013-0538-y.
17. Yaegashi N, Niinuma T, Chisaka H, Uehara S, Moffatt S, Tada K, Iwabuchi M, Matsunaga Y, Nakayama M, Yutani C, Osamura Y, Hirayama E, Okamura K, Sugamura K, Yajima A. 1999. Parvovirus B19 infection induces apoptosis of erythroid cells in vitro and in vivo. J Infect 39:68–76. https://doi.org/10.1016/S0163-4453(99)90105-6.
18. Chen AY, Luo Y, Cheng F, Sun Y, Qiu J. 2010. Bocavirus infection induces mitochondrion-mediated apoptosis and cell cycle arrest at G2/M phase. J Virol 84:5615–5626. https://doi.org/10.1128/JVI.02094-09.
19. Chisaka H, Morita E, Yaegashi N, Sugamura K. 2003. Parvovirus B19 and the pathogenesis of anaemia. Rev Med Virol 13:347–359. https://doi.org/10.1002/rmv.395.
20. Gupta SK, Sahoo AP, Rosh N, Gandham RK, Saxena L, Singh AK, Harish DR, Tiwari AK. 2016. Canine parvovirus NS1 induced apoptosis involves mitochondria, accumulation of reactive oxygen species and activation of caspases. Virus Res 213:46–61. https://doi.org/10.1016/j.virusres.2015.10.019.
21. Poole BD, Zhou J, Grote A, Schiffenbauer A, Naides SJ. 2006. Apoptosis of liver-derived cells induced by parvovirus B19 nonstructural protein. J Virol 80:4114–4121. https://doi.org/10.1128/JVI.80.8.4114-4121.2006.
22. Hsu TC, Wu WJ, Chen MC, Tsay GJ. 2004. Human parvovirus B19 nonstructural protein (NS1) induces apoptosis through mitochondria cell death pathway in COS-7 cells. Scand J Infect Dis 36:570–577. https://doi.org/10.1080/00365540410016230.
23. Morita E, Nakashima A, Asao H, Sato H, Sugamura K. 2003. Human parvovirus B19 nonstructural protein (NS1) induces cell cycle arrest at G(1) phase. J Virol 77:2915–2921. https://doi.org/10.1128/jvi.77.5.2915-2921.2003.
24. Deng X, Xu P, Zou W, Shen W, Peng J, Liu K, Engelhardt JF, Yan Z, Qiu J. 2017. DNA damage signaling is required for replication of human bocavirus 1 DNA in dividing HEK293 cells. J Virol 91: e01831-16. https://doi.org/10.1128/JVI.01831-16.
25. Nuesch JP, Lachmann S, Rommelaere J. 2005. Selective alterations of the host cell architecture upon infection with parvovirus minute virus of mice. Virology 331:159–174. https://doi.org/10.1016/j.virol.2004.10.019.
26. Niskanen EA, Kalliolinna O, Ihalainen TO, Hakkinen M, Vihinen-Ranta M. 2013. Mutations in DNA binding and transactivation domains affect the dynamics of parvovirus NS1 protein. J Virol 87:11762–11774. https://doi.org/10.1128/JVI.01678-13.
27. Cory S, Adams JM. 2002. The Bcll family: regulators of the cellular life-or-death switch. Nat Rev Cancer 2:647–656. https://doi.org/10.1038/nrc883.
28. Ashida H, Mimuro H, Ogawa M, Kobayashi T, Sanada T, Kim M, Sasakawa C. 2011. Cell death and infection: a double-edged sword for host and pathogen survival. J Cell Biol 195:931–942. https://doi.org/10.1083/jcb.201108081.
29. El-Sayed I, Bassiouny K, Nokaly A, Abdelghani AS, Roshdy W. 2016. Influenza A virus and influenza B virus can induce apoptosis via intrinsic or extrinsic pathways and also via NF-kappaB in a time and dose dependent manner. Biochem Res Int 2016:1738237. https://doi.org/10.1155/2016/1738237.
30. Saelens X, Festjens N, Vande Walle L, van Gurp M, van Loo G, Vandenabeele P. 2004. Toxic proteins released from mitochondria in cell death. Oncogene 23:2861–2874. https://doi.org/10.1038/sj.onc.1207523.
31. Iseki H, Shimizukawa R, Sugiyama F, Kunita S, Iwama A, Onodera M, Nakauchi H, Yagami K. 2005. Parvovirus nonstructural proteins induce an epigenetic modification through histone acetylation in host genes and revert tumor malignancy to benignancy. J Virol 79:8886–8893. https://doi.org/10.1128/JVI.79.14.8886-8893.2005.
32. Saxena L, Kumar GR, Saxena S, Chaturvedi U, Sahoo AP, Singh LV, Santra L, Palia SK, Desai GS, Tiwari AK. 2013. Apoptosis induced by NS1 gene of canine parvovirus-2 is caspase dependent and p53 independent. Virus Res 173:426–430. https://doi.org/10.1016/j.virusres.2013.01.020.
33. Kailasan S, Agbandje-McKenna M, Parrish CR. 2015. Parvovirus family conundrum: what makes a killer? Annu Rev Virol 2:425–450. https://doi.org/10.1146/annurev-virology-100114-055150.
34. Chen AY, Zhang EY, Guan WX, Cheng F, Kleiboeker S, Yankee TM, Qiu JM. 2010. The small 11kDa nonstructural protein of human parvovirus B19 plays a key role in inducing apoptosis during B19 virus infection of primary erythroid progenitor cells. Blood 115:1070–1080. https://doi.org/10.1182/blood-2009-04-215756.
35. Mincberg M, Gopas J, Tal J. 2011. Minute virus of mice (MVMp) infection and NS1 expression induce p53 independent apoptosis in transformed rat fibroblast cells. Virology 412:233–243. https://doi.org/10.1016/j.virol.2010.12.035.
36. Op De Beeck A, Sobczak-Thepot J, Sirma H, Bourgain F, Brechot C, Caillet-Fauquet P. 2001. NS1- and minute virus of mice-induced cell cycle arrest: involvement of p53 and p21(cip1). J Virol 75:11071–11078. https://doi.org/10.1128/JVI.75.22.11071-11078.2001.
37. Ohshima T, Yoshida E, Nakajima T, Yagami KI, Fukamizu A. 2001. Effects of interaction between parvovirus minute virus of mice NS1 and coacti-

vator CBP on NS1- and p53-transactivation. Int J Mol Med 7:49–54. https://doi.org/10.3892/ijmm.7.1.49.
38. Nakashima A, Morita E, Saito S, Sugamura K. 2004. Human parvovirus B19 nonstructural protein transactivates the p21/WAF1 through Sp1. Virology 329:493–504. https://doi.org/10.1016/j.virol.2004.09.008.
39. Petrosillo G, Ruggiero FM, Paradies G. 2003. Role of reactive oxygen species and cardiolipin in the release of cytochrome c from mitochondria. FASEB J 17:2202–2208. https://doi.org/10.1096/fj.03-0012com.
40. Shoshan-Barmatz V, Mizrachi D. 2012. VDAC1: from structure to cancer therapy. Front Oncol 2:164. https://doi.org/10.3389/fonc.2012.00164.
41. Nykky J, Vuento M, Gilbert L. 2014. Role of mitochondria in parvovirus pathology. PLoS One 9:e86124. https://doi.org/10.1371/journal.pone.0086124.
42. Deshmane SL, Mukerjee R, Fan S, Del Valle L, Michiels C, Sweet T, Rom I, Khalili K, Rappaport J, Amini S, Sawaya BE. 2009. Activation of the oxidative stress pathway by HIV-1 Vpr leads to induction of hypoxia-inducible factor 1alpha expression. J Biol Chem 284:11364–11373. https://doi.org/10.1074/jbc.M809266200.
43. Kang SM, Kim SJ, Kim JH, Lee W, Kim GW, Lee KH, Choi KY, Oh JW. 2009. Interaction of hepatitis C virus core protein with Hsp60 triggers the production of reactive oxygen species and enhances TNF-alpha-mediated apoptosis. Cancer Lett 279:230–237. https://doi.org/10.1016/j.canlet.2009.02.003.
44. Qi X, Zhang H, Wang Q, Wang J. 2016. The NS1 protein of avian influenza virus H9N2 induces oxidative-stress-mediated chicken oviduct epithelial cells apoptosis. J Gen Virol 97:3183–3192. https://doi.org/10.1099/jgv.0.000625.
45. Chipuk JE, Kuwana T, Bouchier-Hayes L, Droin NM, Newmeyer DD, Schuler M, Green DR. 2004. Direct activation of Bax by p53 mediates mitochondrial membrane permeabilization and apoptosis. Science 303:1010–1014. https://doi.org/10.1126/science.1092734.
46. Adeyemi RO, Pintel DJ. 2012. Replication of minute virus of mice in murine cells is facilitated by virally induced depletion of p21. J Virol 86:8328–8332. https://doi.org/10.1128/JVI.00820-12.
47. Zhang L, Wang ZY, Zhang J, Luo XM, Du Q, Chang LL, Zhao XM, Huang Y, Tong DW. 2018. Porcine parvovirus infection impairs progesterone production in luteal cells through mitogen-activated protein kinases, p53, and mitochondria-mediated apoptosis. Biol Reprod 98:558–569. https://doi.org/10.1093/biolre/ioy014.
48. Brown L, Benchimol S. 2006. The involvement of MAPK signaling pathways in determining the cellular response to p53 activation: cell cycle arrest or apoptosis. J Biol Chem 281:3832–3840. https://doi.org/10.1074/jbc.M507951200.
49. Cargnello M, Roux P. 2011. Activation and function of the MAPKs and their substrates, the MAPK-activated protein kinases. Microbiol Mol Biol Rev 75:50–83. https://doi.org/10.1128/MMBR.00031-10.
50. Perfettini JL, Castedo M, Nardacci R, Ciccosanti F, Boya P, Roumier T, Larochette N, Piacentini M, Kroemer G. 2005. Essential role of p53 phosphorylation by p38 MAPK in apoptosis induction by the HIV-1 envelope. J Exp Med 201:279–289. https://doi.org/10.1084/jem.20041502.
51. Shen W, Deng X, Zou W, Cheng F, Engelhardt JF, Yan Z, Qiu J. 2015. Identification and functional analysis of novel nonstructural proteins of human bocavirus 1. J Virol 89:10097–10109. https://doi.org/10.1128/JVI.01374-15.
52. Tewary SK, Zhao H, Deng X, Qiu J, Tang L. 2014. The human parvovirus B19 non-structural protein 1 N-terminal domain specifically binds to the origin of replication in the viral DNA. Virology 449:297–303. https://doi.org/10.1016/j.virol.2013.11.031.
53. Wang J, Cheng Y, Zhang M, Zhao H, Lin P, Yi L, Tong M, Cheng S. 2015. Development of a nanoparticle-assisted PCR (nanoPCR) assay for detection of mink enteritis virus (MEV) and genetic characterization of the NS1 gene in four Chinese MEV strains. BMC Vet Res 11:1. https://doi.org/10.1186/s12917-014-0312-6.
54. Chen S, Cheng AC, Wang MS, Zhu DK, Jia RY, Luo QH, Cui HM, Zhou Y, Wang Y, Xu ZW, Chen ZL, Chen XY, Wang XY. 2010. Histopathology, immunohistochemistry, in situ apoptosis, and ultrastructure characterization of the digestive and lymphoid organs of new type gosling viral enteritis virus experimentally infected gosling. Poult Sci 89:668–680. https://doi.org/10.3382/ps.2009-00570.
55. Wu X, Wang Z, Zhu D, Zong S, Yang L, Zhong Y, Cui Y. 2013. pH and thermo dual-stimuli-responsive drug carrier based on mesoporous silica nanoparticles encapsulated in a copolymer-lipid bilayer. ACS Appl Mater Interfaces 5:10895–10903. https://doi.org/10.1021/am403092m.